Supporting information: Shoreface dynamics formulation and sensitivity analysis

Lorenzo-Trueba and Ashton

S1. Shoreface dynamics formulation

In this supplementary material, we use a cross-shore energetics sediment transport formulation for wave-driven suspended sediment transport presented by *Ortiz and Ashton* [2013] to develop an analytical estimation for the proposed depth-average shoreface response rate $K\left[L^2/T\right]$. Following the energetics-based approach of *Bowen* [1980], *Ortiz and Ashton* [2013] show that the wave-driven cross-shore suspended sediment transport formulation for shallow-water waves can be formulated as:

$$q_s(z) = -\phi \frac{H(z)^5 g^2}{32 w_s}\left(\frac{15}{4z^3} + \frac{9T^2 g}{16\pi^2 z^4} + \alpha_L(z)\frac{g^{1/2}}{w_s z^{5/2}}\right). \quad \text{(S1)}$$

Under linear Airy wave theory the formulation becomes:

$$q_s(z) = -\phi \frac{\pi^5 H(z)^5}{w_s T^4 \sinh^5(2\pi z/L(z))}\left[\frac{15}{4L(z)} + \frac{9}{4L(z)\sinh^2(2\pi z/L(z))} + \frac{\alpha_L(z)}{w_s T}\right], \quad \text{(S2)}$$

where $z\left[L\right]$ is the local water depth , $T\left[T\right]$ is the wave period, $H\left[L\right]$ the local wave height, $L\left[L\right]$ the local wave length, $w_s\left[L/T\right]$ the settling velocity, $\alpha_L(-)$ the local shoreface slope, $g\left[L/T^2\right]$ the acceleration by gravity, and the coefficient $\phi\left[T^2/L\right]$ is:

$$\phi = \frac{16 e_s C_s \rho}{15\pi(\rho_s - \rho)g}, \quad \text{(S3)}$$

where e_s is the suspended sediment transport efficiency factor, $C_s(-)$ the friction factor, $\rho\left[M/L^3\right]$ the seawater density, and $\rho_s\left[M/L^3\right]$ the sediment density. After rearranging (S1) and

(S2) in the form $q_s(z) = K_L(\alpha_{e,L} - \alpha_L)$, the local, depth-dependent equilibrium slope $\alpha_{e,L}(-)$, and local shoreface response rate $K_L\left[L^2/T\right]$ under the shallow-water waves assumption are:

$$\alpha_{e,L} = \frac{3w_s}{4z^{1/2}g^{1/2}}\left(5 + \frac{3T^2 g}{4\pi^2 z}\right), \tag{S4}$$

$$K_L = \phi\frac{H^5 g^{5/2}}{32w_s^2 z^{5/2}}. \tag{S5}$$

Under linear Airy wave theory the expressions become:

$$\alpha_{e,L} = \frac{3w_s T}{4L}\left(5 + \frac{3}{\sinh^2(2\pi z/L)}\right), \tag{S6}$$

$$K_L = \frac{\phi}{w_s^2}\frac{\pi^5 H^5}{T^5 \sinh^5(2\pi z/L)}. \tag{S7}$$

The local wave height H in (S5) and (S7) can be calculated in terms of the deep wave height $H_0\left[L\right]$ using the standard dispersion relationship.

Using (S3) and (S4) or (S6) and (S7), and assuming the parameter values included in Table S1, the shoreface response rate K_L and the slope α_L as a function of depth in Figure S1. In this paper, however, we conceptualize the shoreface response rate by depth-averaging using the estimation:

$$K = \frac{\int_{z^*}^{D_T} K_L\, dz}{D_T - z^*}, \tag{S9}$$

where the limits of integration are: the shoreface depth D_T, which for our time scale of interest [*Stive et al.*, 1991; *Wright et al.*, 1991; *Stive and de Vriend*, 1995; *Wright*, 1995] is D_T, and the upper limit depth $z^*\left[L\right]$. Note that in the region $0 < z < z^*$, surf-zone processes dominate and the

processes are strongly non-linear and occur on time scales below those of interest here [*Carruthers et al.*, 2013], particularly we are interested in interactions with the deeper shoreface. For the parameter values in Table S1, we obtain $K = 4{,}464\ \mathrm{m^2/y}$ under shallow-water waves, and $K = 1{,}250\ \mathrm{m^2/y}$ under linear Airy wave theory. This motivates our choice to explore barrier dynamics for K spanning the range $0 - 10{,}000\ \mathrm{m^2/y}$.

Table

Table S1. State variables and their dimensions.

Symbol	Meaning	Value
T	wave period	8 s
H_0	deep wave height during fair weather	1 m
w_s	settling velocity	0.033 m/s
g	gravity	9.8 m/s^2
e_s	suspended sediment transport efficiency factor	0.01
C_s	friction factor	0.01
ρ	seawater density	1,040 kg/m^3
ρ_s	sediment density	2,650 kg/m^3
z^*	Upper limit depth	5 m
D_T	shoreface depth	15 m

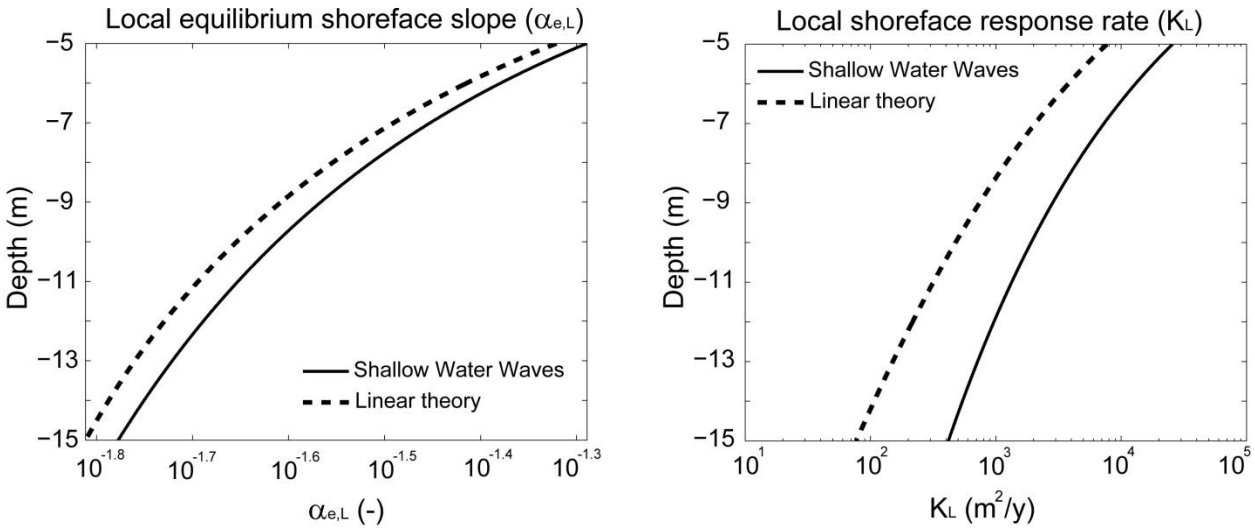

Figure S1. Plots of the local equilibrium slope $\alpha_{e,L}$, and the local shoreface response rate K_L as a function of water depth z.

S2. Sensitivity to initial conditions:

All the results presented in the main manuscript assume that the initial barrier geometry is at static equilibrium (equation (29) in the main text). In this section, we investigate different initial conditions, finding that this assumption plays a minor role on the type of barrier response. In particular, we find that independently of the initial conditions the system eventually attains a constant amplitude and frequency of oscillation (Figure S2).

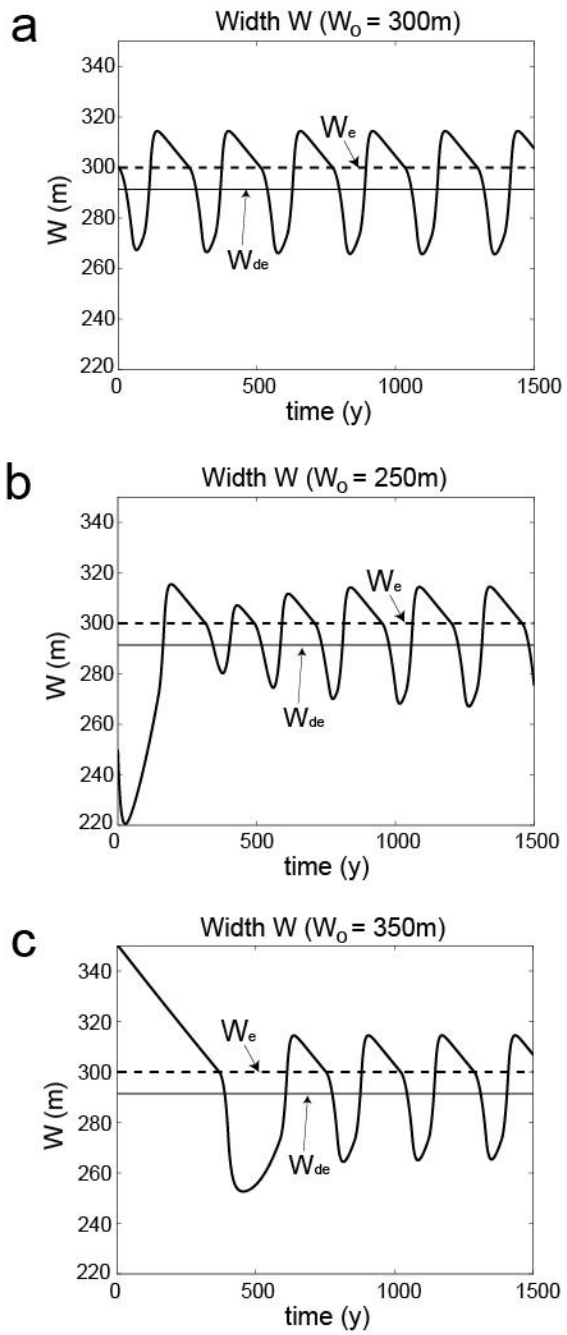

Figure S2. Time evolution of the barrier width for a barrier system undergoing 'periodic retreat' for different initial barrier widths. The input parameter values are included in Table S2, and the initial conditions in Table S3.

S3. Sensitivity analysis to input parameters:

Changes in the sea-level rise rate and the bathymetric profile landward of the subaerial barrier back-barrier slope play a major role on the type of barrier response, as discussed in the main text (Figures 11 and 12). In this supplementary material, for completeness we present results from sensitivity analyses focusing on parameters found to play a minor role in the type of barrier response. These are the maximum deficit volume $V_{d,\max}$, shoreface toe depth D_T, equilibrium (or critical) barrier width W_e and height H_e, and equilibrium (or critical) shoreface slope α_e.

3.1 Maximum deficit volume

A change in the maximum deficit volume $V_{d,\max}$ has a minor effect on the height and width drowning regions, but it enhances dynamic equilibrium in lieu of discontinuous retreat (Figure S3).

3.2 Shoreface Toe Depth

The depth of the shoreface toe D_T is directly linked to wave, climate, sediment size, and the time scale under consideration [*Stive and de Vriend*, 1995; *Cowell et al.*, 1999]. Given the simple geometry of a constant slope continental shelf, as we increase D_T, we concomitantly increase the back-barrier depth. By increasing the accommodation depth, this results in a reduction of the efficiency of the overwash flux and a reduction of the shoreface response rate. Thus, if we doubled D_T, maintaining the same barrier response would require doubling the amount of overwash and shoreface response rate (Figure S4).

2.3 Critical barrier width

As we might expect, narrow barriers are more prone to width drowning (Figure S5). Beyond a threshold barrier width, however, changes in W_e have little effect on barrier response.

2.4 Critical height and shoreface slope

Changes in H_e (Figure S6) or α_e (Figure S7) have only a modest effect on barrier response.

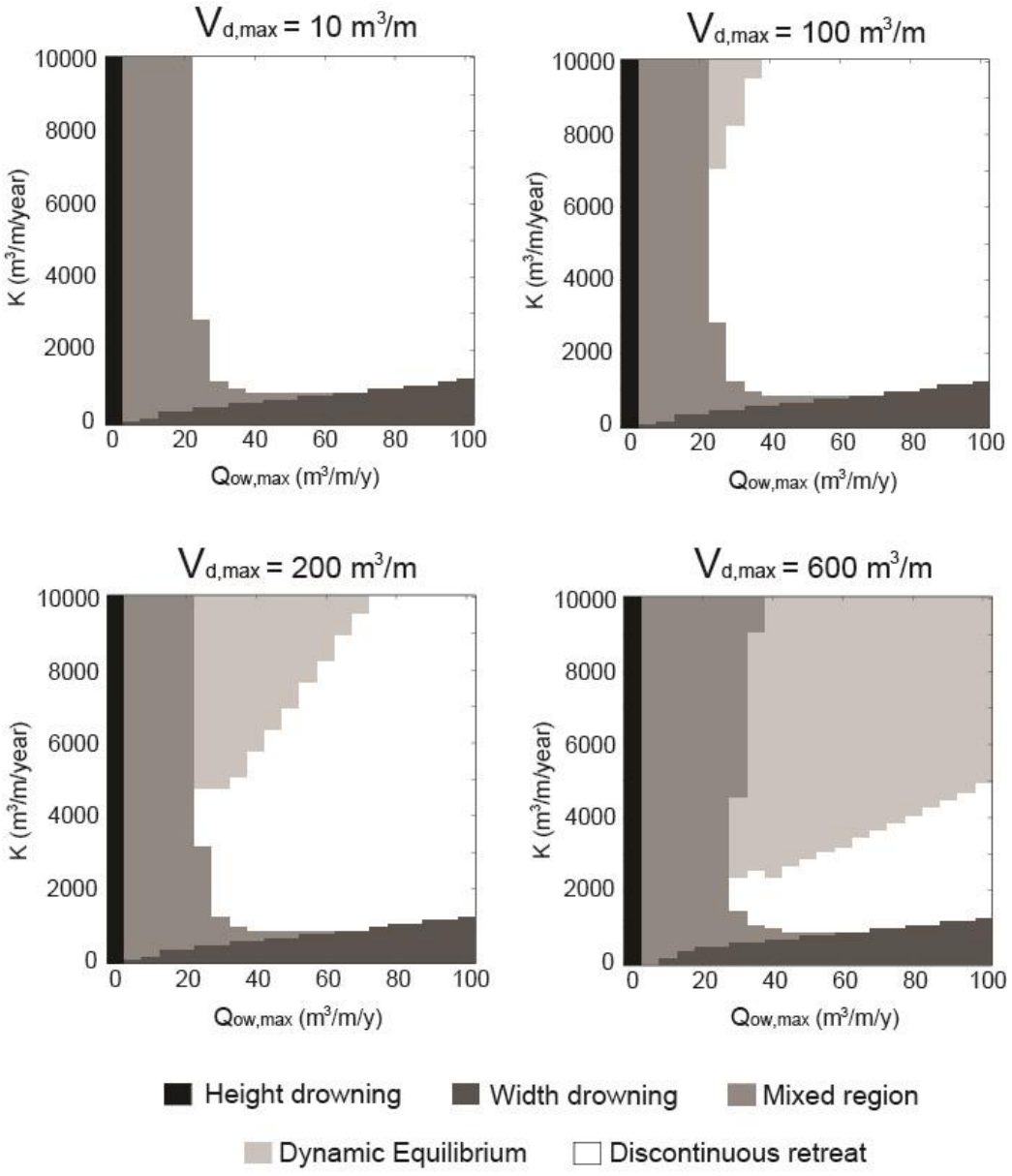

Figure S3. Phase diagrams of barrier evolution type for different values of the maximum deficit volume $V_{d,\max}$. Parameter values are included in Table S2.

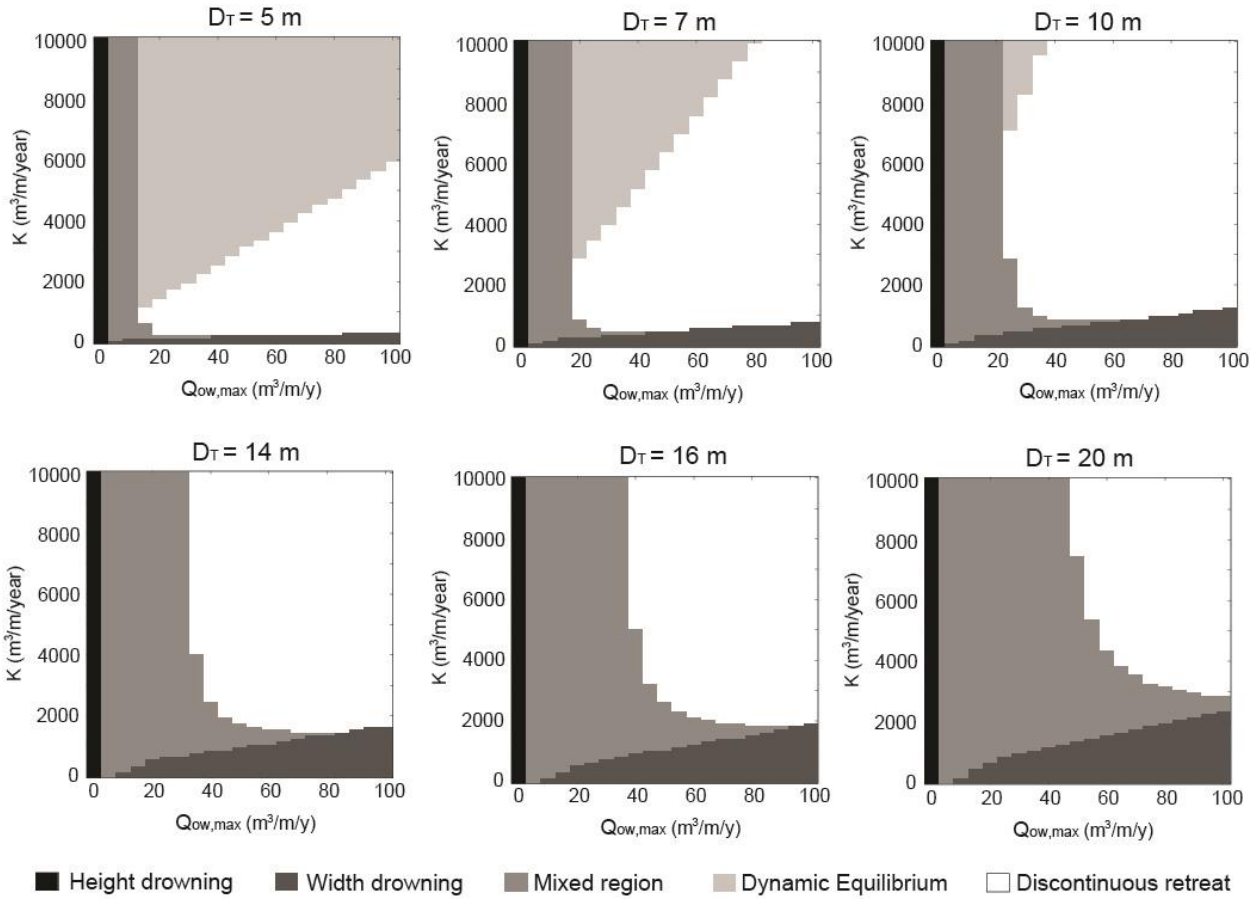

Figure S4. Phase diagrams of barrier evolution type for different values of the shoreface toe depth D_t. Note that an increase in D_t reduces the efficiency of $Q_{OW,\max}$ and K. For instance, the $D_t = 20\,\mathrm{m}$ regime diagram 'zooms' into region of the $D_t = 10\,\mathrm{m}$ regime diagram, within the range $Q_{OW,\max} = (0 - 50\,\mathrm{m^3/m/y})$ and $K = (0 - 5{,}000\,\mathrm{m^3/m/y})$. Parameter values are included in Table S2.

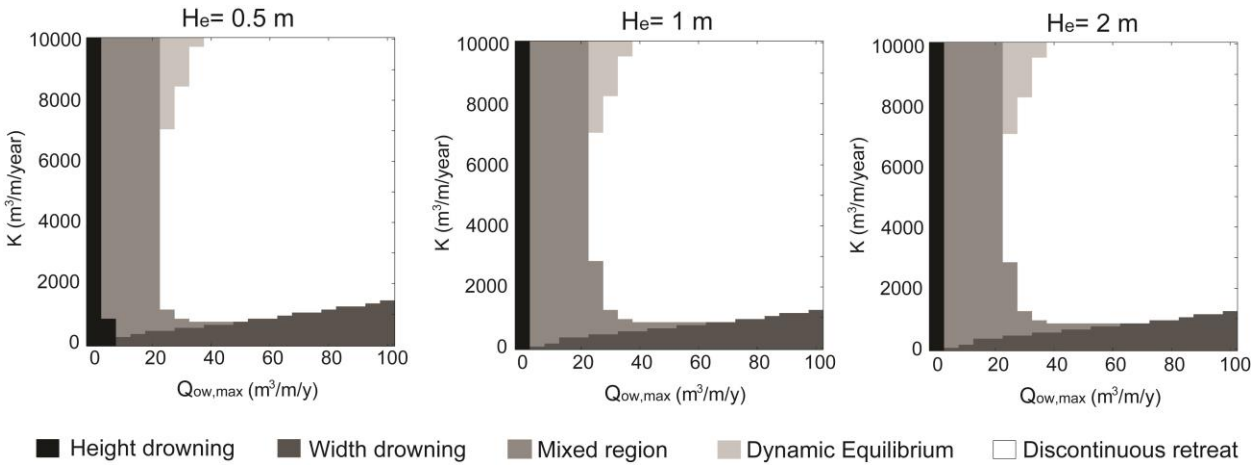

Figure S5. Phase diagrams of barrier evolution type for different values of the critical (or equilibrium) height H_e. Parameter values are included in Table S2.

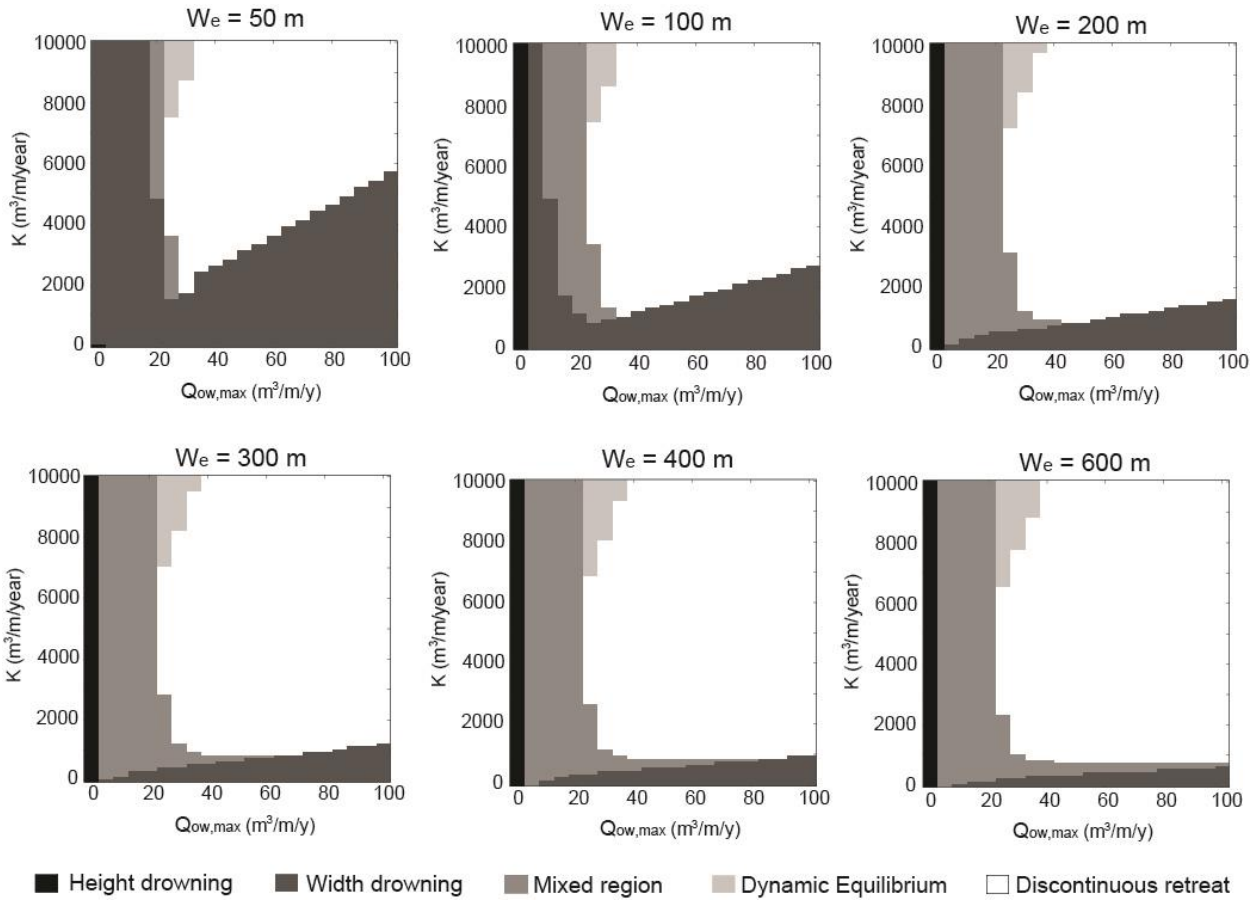

Figure S6. Phase diagrams of barrier evolution type for different values of the critical (or equilibrium) width W_e. Parameter values are included in Table S2.

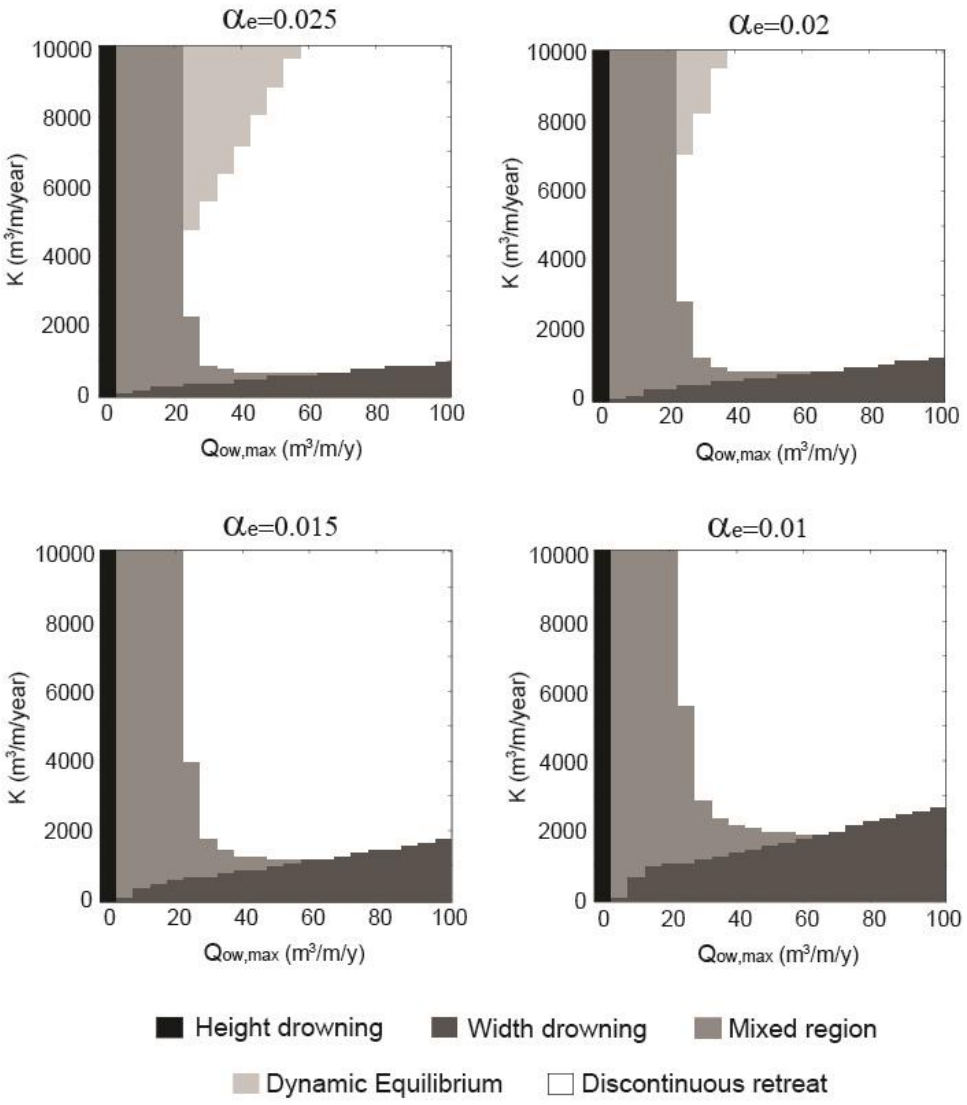

Figure S7. Phase diagrams of barrier evolution type for different values of the equilibrium shoreface slope α_e. Parameter values are included in Table S2.

Table S2. Input parameters used in Figures S2 to S7.

Figure	K $(m^3/m/y)$	$Q_{OW,\max}$ $(m^3/m/y)$	$V_{d,\max}$ (m^3/m)	α_e $(-)$	β $(-)$	W_e (m)	H_e (m)	D_T (m)	$\dot{z}$ (mm/y)
S2	5,000	70	300	0.02	0.001	300	2	10	2
S3	*varies*	*varies*	*varies*	0.02	0.001	300	2	10	2
S4	*varies*	*varies*	100	0.02	0.001	300	2	*varies*	2
S5	*varies*	*varies*	100	0.02	0.001	300	*varies*	10	2
S6	*varies*	*varies*	100	0.02	0.001	*varies*	2	10	2
S7	*varies*	*varies*	100	*varies*	0.001	300	2	10	2

Table A3. Initial Conditions.

Figure	α_0 $(-)$	W_0 (m)	H_0 (m)
S2a	α_e	W_e	H_e
S2b	α_e	250	H_e
S2c	α_e	350	H_e

References

Bowen, A. J. (1980), Simple models of nearshore sedimentation: Beach profiles and longshore bars, in *The Coastline of Canada*, edited by S. B. McCann, pp. 1-11, Geological Survey of Canada, Ottawa, Ontario.

Carruthers, E. A., D. P. Lane, R. L. Evans, J. P. Donnelly, and A. D. Ashton (2013), Quantifying overwash flux in barrier systems: an example from Martha's Vineyard, Massachusetts, USA, *Mar. Geol.*

Cowell, P. J., D. J. Hanslow, and J. F. Meleo (1999), The Shoreface, in *Handbook of Beach and Shoreface Morphodynamics*, edited by A. D. Short, pp. 39-71, John Wiley & Sons.

Ortiz, A. C., and A. Ashton (2013), A Morphodynamic Explanation for the Shoreface Depth of Closure, *8th Symposium on River, Coatal and Estuarine Morphodynamics*.

Stive, M. J. F., and H. J. de Vriend (1995), Modelling shoreface profile evolution, *Mar. Geol.*, *126*(1–4), 235-248.

Stive, M. J. F., R. J. Nicholls, and H. J. deVriend (1991), Sea-level rise and shore nourishment - a discussion, *Coast Eng.*, *16*(1), 147-163.

Wright, L. D. (1995), *Morphodynamics of inner continental shelves*, 241 pp., CRC Press, Boca Raton.

Wright, L. D., J. D. Boon, S. C. Kim, and J. H. List (1991), Modes of cross-shore sediment transport on the shoreface of the Middle Atlantic Bight, *Mar. Geol.*, *96*(1-2), 19-51.